Effect of injection timing on mixture formation and combustion in an ethanol direct injection plus gasoline port injection (EDI+GPI) engine

Yuhan Huang [a,b *], Guang Hong [a], Ronghua Huang [b]

Affiliations:

[a] School of Electrical, Mechanical and Mechatronic Systems, University of Technology Sydney, Sydney, Australia

[b] State Key Laboratory of Coal Combustion, Huazhong University of Science and Technology, Wuhan, China

Corresponding author:

Yuhan Huang, PhD student

Postal address: School of Electrical, Mechanical and Mechatronic Systems, University of Technology Sydney, PO Box 123, Broadway NSW 2007, Australia

Email: Yuhan.Huang@student.uts.edu.au

Telephone: +61 415040942

Abstract

Ethanol direct injection plus gasoline port injection (EDI+GPI) is a new technology to utilise ethanol fuel more effectively and efficiently in spark-ignition engines by taking the advantages of ethanol fuel and direct injection, such as the cooling effect and anti-knock ability. A full cycle numerical modelling including both port and direct injection sprays was performed to understand the mechanisms behind the experimental results of the EDI+GPI engine. The turbulence-chemistry interaction of the two-fraction-mixture partially premixed combustion was solved by a five-dimensional presumed Probability Density Function table. Effects of direct injection timing on fuel evaporation, mixing, wall-wetting, combustion and emission processes were investigated. The results showed that when the direct injection timing was retarded, the mixture around the spark plug became leaner and the distribution of equivalence ratio became more uneven. Moreover, late direct injection resulted in severe fuel impingement and caused local over-cooling effect and over-rich mixture. Consequently, the combustion speed and temperature were decreased by retarded direct injection timing, leading to reduced NO emission and increased HC and CO emissions. Finally, numerical modelling was performed to investigate the strategy of injecting small amount of ethanol fuel on reducing the fuel impingement and incomplete combustion caused by late direct injection.

Keywords:

Ethanol direct injection; Gasoline port injection; Dual-fuelled; Numerical modelling; Injection timing

1. Introduction

Driven by financial incentives and renewable energy policies, ethanol fuel is becoming more and more popular globally in recent years. The global consumption of ethanol fuel has increased from 4.5 billion gallons in 2000 to 21.8 billion gallons in 2012 [1]. Ethanol fuel is usually used as a substitute or octane-enhancer for gasoline fuel in spark ignition (SI) engines. Ethanol can be used as neat fuel or blended fuel with gasoline in SI engines. The performance of engines fuelled with neat ethanol fuel was investigated [2-4]. The results showed the advantages of using pure ethanol fuel in the tested conditions. However, as neat fuel, ethanol may be not suitable to power SI engines in some conditions because of its low volatility, low heating value and high enthalpy of vaporization, especially under cold conditions [5-7]. At present, therefore, ethanol is mostly used via blending with gasoline fuel, such as E10 (gasoline containing 10% of ethanol by volume) for commercial passenger cars and E85 (gasoline containing 85% of ethanol by volume) for flexible-fuel vehicles (FFV). Many studies have been conducted in this field. Karavalakis et al. [8] measured the gaseous and particulate emissions of spray-guided and wall-guided DI SI engines fuelled with ethanol/gasoline and iso-butanol/gasoline blends. Ozsezen et al. [9] investigated the performance of a vehicle fuelled with 5% and 10% alcohol/gasoline blends. Suarez-Bertoa et al. [10] measured the regulated and unregulated emissions from a Euro 5a FFV fuelled with different gasoline/ethanol blends. Turner et. al. [11] investigated the combustion performance of a DI SI engine with various ethanol/gasoline blending ratios. The results showed that blending ethanol with gasoline reduced emissions and increased efficiency, and the impact changed with the blending ratio.

Blending ethanol with gasoline at a fixed ratio limits ethanol's potentials in improving the engine performance over the wide engine operation conditions. To make the use of ethanol fuel more flexible and efficient, a dual-injection system was developed, which combined the advantages of port injection (PI) and direct injection (DI). Dual-injection concept has been intensively investigated in compression ignition (CI) engines. For example, to reduce the NOx and soot emissions by reducing in-cylinder temperature, water was injected by a PI system whilst diesel was supplied in a separate DI system [12-14]. Water PI was used to enhance the hydrogen energy share in a diesel DI engine [15]. Recently, a dual-injection strategy called Reactivity Controlled Compression Ignition (RCCI) was developed for CI engines, in which a lower reactivity fuel (e.g., gasoline) was supplied via PI and a more reactive fuel (e.g., diesel) was supplied via DI [16-19]. Although dual-injection has been investigated in CI engines, the application of dual-injection concept in SI engines is relatively new. Cohn et al. firstly proposed to use ethanol DI in a downsized, highly turbocharged and high compression ratio gasoline PI engine [20]. The engine efficiency was predicted to be greatly increased by using a small amount of ethanol fuel with engine downsizing technologies. Toyota developed a D-4S (Direct injection 4-stroke gasoline engine system Superior version) engine equipped with a PI injector and a DI injector [21]. The gasoline PI is applied in part load and the gasoline DI is applied in full load. By doing so, the compression ratio of the D-4S engine has been increased to 12.7 in production

cars [22]. Following the dual-injection concepts of MIT and Toyota, many studies have been carried out. Ford introduced the "EcoBoost" engine in the 2010 Lincoln MKS [23]. The gasoline is used via PI and E85 is used via DI. The "EcoBoost" engine showed significant leveraging effect of E85 on reducing the gasoline fuel consumption and CO_2 emission. Zhu et al. [24] investigated the combustion characteristics of an engine fuelled by three injection strategies, including gasoline PI plus gasoline DI, gasoline PI plus E85 DI, and E85 PI plus gasoline DI. Recently, Wang et al. [25] compared the engine performance of alcohols-gasoline (alcohols PI plus gasoline DI) and gasoline-alcohols (gasoline PI plus alcohols DI) dual-fuel spark ignition (DFSI) systems. The results in [24] and [25] showed that the engines fuelled by gasoline PI plus alcohols DI demonstrated higher efficiency than other injection strategies because alcohols DI better utilized the high enthalpy of vaporization of alcohol fuels. Wu et al. [26] tested the dual-injection concept of gasoline PI plus ethanol or DMF DI as a flexible way to utilise bio-fuels. The leveraging effect of using ethanol fuel on reducing gasoline fuel consumption in an ethanol DI plus gasoline PI (EDI+GPI) engine was experimentally studied [27]. The combustion and emission characteristics of an ethanol PI and gasoline DI engine was investigated, which aimed to utilise the charge cooling effect of both gasoline and ethanol fuels [28]. The anti-knock ability [29-31] of the dual-injection concept of alcohols DI plus gasoline PI was experimentally investigated.

The experiments reviewed above have shown the advantages of EDI+GPI over the conventional single injection fuel system in terms of engine performance. To understand the mechanisms behind the experimental results and further exploit ethanol's potentials, the in-cylinder flows, fuel evaporation and mixing, combustion and emission processes need to be investigated. The combustion characteristics of gasoline PI plus ethanol or DMF DI dual-injection were investigated in an optical engine [32]. The results showed that gasoline-ethanol dual-injection had faster combustion speed than that of gasoline PI. Computational fluid dynamics (CFD) modelling has been proven a feasible and economic tool to get the visualised in-cylinder flows and thus shorten the research cycle [33]. So far, however, only a few publications were found on the spray combustion modelling of dual-injection systems. Yang et al. [34] numerically studied the dual-injection combustion mode with gasoline PI plus diesel DI. The combustion process of in-cylinder fuel blending by gasoline PI plus early diesel DI was modelled [35]. The reactivity gradient of a dual fuelled engine with gasoline PI plus diesel DI was numerically investigated [36]. Lu et al. [37] simulated the combustion and emission processes of a dual-fuel sequential combustion (DFSC) engine with n-heptane PI plus iso-octane DI. The effects of DI strategy on a diesel DI plus natural gas PI RCCI engine was numerically studied [38]. The simulations in the above reviewed studies did not include the fuel port injection process. Instead the port injected fuel was assumed to be homogenous in the combustion chamber before combustion or intake valve close. However, experimental and numerical results showed that the fuel was not fully evaporated as excepted or evenly distributed in the combustion chamber for the port injected gasoline spray [39-41].

As reviewed above, following the demonstration of advantages of EDI+GPI, it is needed to investigate the in-cylinder flow details of EDI+GPI dual-injection by CFD simulation. However little numerical study has been reported to investigate the mixture formation and combustion characteristics of the dual-injection system considering both the port injection and direct injection sprays. Modelling spray combustion of EDI+GPI is challenging because it is a typical example of partially premixed SI combustion and the distributions of the two fuels at each computational grid vary. As a result, solving spray combustion fields of two fuels simultaneously can be much more computationally expensive than that of single injection system [40]. The present work investigated the fuel evaporation, mixing, wall-wetting, combustion and emission characteristics of an EDI+GPI dual-fuelled research engine in a full engine cycle CFD simulation. The two-fraction-mixture combustion of dual-injection was modelled by combining the ECFM partially premixed combustion model with a five-dimensional double-delta PDF look-up table. CFD simulations were carried out to understand the mechanisms associated with the experimental results and investigate potential ideas that may improve the engine performance, which could not be experimentally implemented on the current engine.

2. CFD modelling

2.1. 3D Engine model

The three-dimensional CFD simulations were performed in the ANSYS FLUENT code environment. The in-cylinder flows were modelled by the Realizable k-ε turbulence model. A number of sub-models were used to simulate the various physical and chemistry processes in the combustion chamber, including the droplet break-up, evaporation, distortion and drag, wall-film, combustion and emission formation, as listed in Table 1. The dual-fuel spray was modelled using the Eulerian-Lagrangian approach which was based on the Monte-Carlo statistical method. The continuous gas phase was treated using the Eulerian method whilst the dispersed spray droplets were tracked in the Lagrangian method. The spray was represented by a number of discrete parcels. Each parcel contained a group of identical non-interacting droplets. By solving the ordinary differential equations for the trajectory, momentum, heat and mass transfer of a single droplet, it solved the equations for many droplets in the whole parcel. The interactions between the gas and liquid phases were taken into account by the source terms in the partial differential equations of the gas phase. Obviously, the larger the number of the parcels was, the more accurate of the representation for the spray behaviours was [42, 43]. Therefore 20 parcels per hole were released at the nozzle exit in each time step in the present study. The total number of parcels introduced into the computational domain was around 9000 for gasoline spray and 30000 for ethanol spray. The Rosin-Rammler Diameter Distribution Method was used to model the primary breakup process (blob injection concept) [44]. It was based on the assumption that an exponential relationship existed between the droplet diameter (d) and the mass fraction of droplets with diameter greater than d. The consequent droplets breakup process was modelled by the WAVE model

[45]. WAVE model was appropriate for high Weber number (*We* >100) flows, which considered the breakup of the droplets to be induced by the relative velocity between the gas and liquid phases [46, 47]. Although the initial velocity of the low pressure (0.25 MPa) GPI spray was relatively slow, the air velocity in the intake manifold could be as high as 200 m/s, as shown in Fig. 5. As a result, the *We* numbers for both the EDI and GPI droplets were greater than 100. The droplet distortion and drag were taken into account by the Dynamic Drag model [48]. It assumed that the droplet drag coefficient was related to the magnitude of the drop distortion. The droplet-wall interaction model was based on the work of Stanton [49] and O'Rourke [50]. A liquid droplet may stick, rebound, spread or splash when it collides with a wall, depending on the impact energy and wall temperature. The Convection/Diffusion Controlled Model [51] was adopted to model the evaporation process of ethanol and gasoline sprays. It takes into account the effects of gradient diffusion and convection on the droplet evaporation.

The spray evaporation model provided the combustion model with the amount and distribution of vapour fuel for each fuel. The combustion process was initiated in the Zimont model by releasing a specific amount of energy to the cells at the spark plug gap [47]. The flame kernel increased from an initial radius 2 mm to the final radius 5 mm with a time exponent of 1/3. Spray combustion in DI SI engines was a typical example of partially premixed combustion because the mixture was not perfectly homogeneous and evaporating and mixing processes were still occurring by the time of ignition. Therefore, the consequent dual-fuel combustion process was modelled by the Extended Coherent Flame Model (ECFM) with the partially premixed combustion concept, in which both the progress variable c and the mixture fraction Z were solved [40]. The Coherent Flame Model (CFM) was based on the assumption that the chemical time scales were much smaller than the turbulence time scales, which was applicable for both premixed and non-premixed internal combustion engine conditions. The ECFM model was the extension of the CFM and aimed to be able to simulate the stratified spray combustion conditions [52]. It was mainly developed for DI SI engines. The ECFM combustion model was properly tuned by acting on the intermediate turbulent net flame stretch (ITNFS) term so that the modelled in-cylinder pressure traces matched the experimental data. The laminar flame speeds of ethanol and gasoline fuels were taken from the experiments [53]. The turbulent flame speed was calculated based on the laminar flame speed and the local turbulence intensity in the combustion model. The NO formation was model by the Extended Zeldovich mechanism [54]. To model the turbulence-chemistry interactions of the two-fraction mixture, a five-dimensional double-delta Probability Density Function (PDF) table was generated to take into account the two fuels. The chemistry look-up table was generated using complex reaction mechanisms which incorporated the latest insights on combustion chemical kinetics [55]. The instantaneous scalar values (species mass fractions, density and temperature) were calculated as a function of the first fuel mixture fraction, the secondary fuel partial fraction and the normalized heat loss/gain before the calculation. These information were stored in the five-dimensional PDF look-up table. The mean values of mass fractions, density and temperature in each cell of the computational domain were obtained by interpolation during the calculation.

The computational mesh was generated based on the geometry scanned from the cylinder head of the EDI+GPI engine. As shown in Fig. 1, the mesh includes the geometry details of the combustion chamber, valves, spark plug, intake manifold with the throttle plate, and the exhaust manifold. The GPI injector was installed after the throttle plate and the EDI injector was mounted 15 mm to the spark plug on the intake valve side. The number of grids were 178887 at the start of calculation (410 CAD BTDC). The mesh density independence study was carried out in a previous study [40]. The simulation started from the GPI injection (410 CAD BTDC) and ended at the exhaust top dead centre (360 CAD ATDC). To reduce the computation time, the grids for the intake or exhaust port were deactivated when the valve was closed.

2.2. Model verification

Fig. 2 shows the comparison between the simulated and measured in-cylinder pressure traces at different EDI timings at the engine speed of 4000 rpm. The good agreement, including the peak pressure value and its phase, illustrates that the engine model is valid for investigating the effect of EDI timing on the EDI+GPI dual-fuel mixture formation and combustion processes.

2.3. Engine setup and simulation conditions

The EDI+GPI engine to be modelled is a single-cylinder air-cooled SI engine [27]. Table 2 lists the engine specifications. The EDI+GPI dual-injection fuel system offers the flexibility to change the ethanol/gasoline ratio according to the engine conditions. Table 3 gives the engine conditions investigated in the present study. Three EDI timings at different regions were tested, including early EDI timing during the intake stroke at 300 CAD BTDC (IT300), medium EDI timing at 180 CAD BTDC (IT180) and late EDI timing during the compression stroke at 100 CAD BTDC (IT100). The mixture was stoichiometric and ethanol/gasoline ratio was fixed at 46% by volume (8.5 mg gasoline PI + 8.0 mg ethanol DI). The GPI timing was 410 CAD BTDC and the spark timing was 15 CAD BTDC. The injection pressure was 0.25 MPa for GPI and 6.0 MPa for EDI. The effect of direct injection of small amount of ethanol fuel at 25% and 10% on reducing the wall-wetting and incomplete combustion of late EDI timing at 100 CAD BTDC was also investigated.

3. Results and discussion

In the development of EDI+GPI, late EDI timing is desired because late EDI timing is more effective than early EDI timing on knock mitigation. Experimental results showed that late EDI timing allowed more advanced spark timing without knock issue than early EDI timing did, but also deteriorated the combustion and emission performance of the engine [31]. As shown in Fig. 2, the peak cylinder pressure decreases with the retarded EDI timing. The measured CO and HC emissions increase and IMEP and NO emission decrease when EDI timing is retarded, as shown in Fig. 3. The present study aims to understand the mechanisms behind the experimental results by CFD simulation. The following sections will present and discuss the

effect of injection timing on the mixture formation, wall-film, combustion and emission processes of the EDI+GPI engine in the experimentally tested conditions. Based on that, the potential of direct injection of small amount of ethanol fuel that cannot be realised on the current research engine on reducing the wall-wetting and incomplete combustion has been examined.

3.1. Effect of EDI timing on mixture formation

Fig. 4 shows the variations of the mass of evaporated ethanol fuel with crank angle degrees (CAD) from intake top dead centre (TDC) to exhaust valve open (EVO). As shown in Fig. 4, the mass percentage of evaporated ethanol fuel at spark timing decreases from 93.4% (7.47mg/8.00mg) in IT300 condition to 89.4% (7.16mg/8.00mg) in IT180 condition and 44.8% (3.583mg/8.00mg) in IT100 condition. This is because the flow field is less intensive in the compression stroke and the time is shorter for the fuels to evaporate and to mix with air with retarded EDI timing. As introduced in Section 2.1, the Convection/Diffusion Controlled model [51] is used to simulate the evaporation processes of gasoline and ethanol droplets in the present study. The gradient diffusion effect is governed by the fuel saturation vapour pressure and the convection effect is governed by the flow velocity. In high-velocity flows, the effect of convective flow on taking the evaporating material from the droplet surface to the bulk gas phase becomes significant. Fig. 5 shows the in-cylinder flow velocity vectors at the start and the end of the EDI injection of different injection timings. As shown in Fig. 5, for IT300 condition, the intake valve is fully open and the intake flow rate is as high as 200 m/s. This high flow rate increases the heat and mass transfer between the fuel droplets and the ambient gas, thus accelerates the fuel evaporation and enhances the mixing. The in-cylinder flows become much slower in the compression stroke. This leads to the low evaporation rate of ethanol fuel at retarded EDI timings of IT180 and IT100. Particularly, the intake gas flow rate reduces significantly from 150 m/s at the start of EDI injection to 90 m/s at the end of EDI injection for IT180 due to the intake valve closing, as shown in Fig. 5. This significant change in velocity may lead to the fluctuation of IMEP when EDI timing is between 120 and 250 CAD BTDC in the engine experiments, as reported in [31]. The lower evaporation rate of late EDI injection has significant effect on the following combustion process. As the EDI timing retards, the combustion speed becomes slower to propagate to the regions with too-rich and over-cooled mixture (which will be discussed in Fig. 10). As a result, after the combustion takes place, both the gasoline and ethanol vapour fuels are burnt/consumed more slowly in IT180 and IT100 than that in IT300, as shown in Fig. 4. By the time of EVO, there are 0.018 mg (0.21%) unburnt gasoline and 0.041 mg (0.51%) unburnt ethanol in the IT300 condition. The unburnt gasoline and ethanol fuels increase to 0.504 mg (5.93%) and 2.196 mg (27.45%) respectively in IT180 condition and 0.340 mg (4.00%) and 2.081 mg (26.01%) in IT100 condition. These unburnt fuels contribute to the increased HC emission in the engine experiments, as discussed in Section 3.3.

Fig. 6 shows the spatial mass distributions of gasoline and ethanol vapours and the equivalence ratio on a vertical plane passing through the spark plug by spark timing. With retarded EDI timing, the gasoline fuel

becomes leaner in the left side of the combustion chamber because more ethanol fuel is vaporised in this region, which consequently cools this region and slows down the gasoline evaporation. As the EDI timing retards, the ethanol droplets have less time to interact with the intake swirls which would entrain the ethanol fuel to the right region of the combustion chamber. As a result, the ethanol mass fraction becomes leaner in the right side, but richer in the left side. With the retarded EDI timing, the mixture around the spark plug becomes leaner from 0.83 equivalence ratio in IT300 condition to 0.67 in IT180 condition and 0.68 in IT100 condition. This leads to longer combustion initiation duration, slower flame propagation speed and difficulty for the flame to reach the near wall regions. Consequently it reduces the peak cylinder pressure and combustion temperature and increases the HC and CO emissions. This will be further discussed in Section 3.3.

3.2. Effect of EDI timing on fuel impingement

Fig. 7 shows the variation of wall film mass with crank angle degrees at the EDI timings of 300, 180 and 100 CAD BTDC. As shown in Fig. 7, the fuel impingement on the cylinder and piston walls becomes severer when EDI timing is retarded from 300 to 180 and then to 100 CAD BTDC. At the EDI timing of 300 CAD BTDC (during the intake stroke), the intake air flow rate is high and the piston is moving downward, as shown in Fig. 5. The ethanol droplets are being entrained into the intake air swirls. This avoids the ethanol spray collision on the cylinder and piston walls. When EDI timing is retarded to be in the compression stroke (IT180 and IT100), the volume of the combustion chamber becomes smaller and the in-cylinder flow rate reduces. However, the in-cylinder pressure during the IT180 and IT100 spray injections does not increase significantly when EDI timing is retarded from 300 to 100 CAD BTDC, as shown in Fig. 2. As a result, the ethanol droplets reach the cylinder and piston walls more easily at late EDI timings, causing severer fuel impingement. Moreover, at early EDI timing of 300 CAD ATDC, the wall film has more time to absorb the heat from the hot cylinder walls and evaporate before the combustion takes place. While the wall film formed in IT180 and IT100 conditions does not have enough time to evaporate by the time of spark timing, as shown in Fig. 7. The increased wall film becomes another import source for the formation of HC emission of late EDI timing conditions.

3.3. Effect of EDI timing on combustion and emissions

Fig. 8 shows the distributions of flame-brush on a plane cutting through the spark plug varing with the crank angle degree at different EDI timings and Fig. 9 shows the corresponding distributions of combustion temperature. In the modellling of premixed combustion, progress variable c is introduced to describe the state of the reactants, where $c=0$ stands for fresh mixture and $c=1$ is for burnt mixture. A value between 0 and 1 indicates the flame-brush. Fig. 8 shows that the ignition flame kernel is well formed at 5 CAD ATDC in IT300 condition but still very small in IT180 and IT100 conditions, demonstrating a shorter combustion initiation duration of IT300 than that of IT180 and IT100. The calculated combustion initation duration

(CA0-10%) from the measured cylinder pressure increased from 20.7 CAD in IT300 to 24.3 CAD in IT180 and 24.8 CAD in IT100. Consistently the flame propagates much faster in IT300 than that in IT180 and IT100. This is because the mixtures are leaner in IT180 and IT100 due to the less intensive in-cylinder flows and less time for ethanol to evaporate and to mix with the air, as shown in Figs. 4 and 5. The flame speed and combustion temperature reach their peaks at the stoichiometric equivalence ratio. Either lean or rich mixture results in much lower combustion speed and temperature [53, 56]. Consequently, as shown in Fig. 9, the combustion temperature is much lower in IT180 and IT100 conditions than that in IT300 condition. Particularly, the temperature in the region next to the spark plug is relatively high (~2500K) in IT300 condition. This is because this region has equivalence ratio closer to 1, as shown in Fig. 6. This higher temperature region is also the main place for the NO formation, as shown in Fig. 11 which will be discussed later.

Fig. 10 shows the distributions of flame brush, ethanol droplets, equivalence ratio and combustion temperature on a horizontal plane under the spark plug at EVO. Compared with IT300 condition, there are larger unburnt regions in IT180 and IT100 conditions. This is caused by the fuel not evaporated yet and poor quality of mixture at late EDI injection, resulting in a large proportion of unevaporated ethanol droplets during the combustion and uneven distribution of equivalence ratio. Fig. 10 shows clearly that the regions in which the flame cannot propagate to are the regions where the ethanol droplets concentrate at. By the time of spark, 6.6% of ethanol fuel remains unevaporated in IT300 condition, 10.6% in IT180 and 55.2% in IT100 (Fig. 4). As the flame propagating, most of the ethanol droplets have evaporated and been burnt by the time of EVO at IT300. However, as shown in Fig. 10, there are still some ethanol droplets remaining in the near wall regions with late EDI injections of IT180 and IT100. The high ethanol droplet concentration deteriorates the combustion process in two ways. Firstly, as shown in Fig. 10, the ethanol droplets evaporate and lead to very rich mixture in the high concentration regions. When the equivalence ratio is higher than 2.0, the flame speed becomes very slow [53]. Secondly, the over-cooling effect becomes significant with late EDI injections. When ethanol droplets evaporate in the high concentration regions, they need a large amount of thermal energy for the phase change. This results in over-cooling effect in the corresponding regions. As shown in Fig. 10, larger regions in IT180 and IT100 conditions have been cooled to as low as 400 K. Such a low temperature makes it more difficult for the flame to reach these regions.

Fig. 11 shows the spatial distribution of the NO concentration at EVO. The formation of thermal NO is a result of high temperature (>1800K) and rich oxygen concentration. As shown in Fig. 11, the high temperature regions shown in Fig. 9 have the highest NO concentrations. The formation of NO emission becomes less intensive with the retarding of the EDI timing because of the reduced cylinder temperature. As shown in Fig. 3, the measured indicated specific NO emission decreased from 10.14 g/kw-h in IT300 condition to 7.76 g/kw-h in IT180 condition and 6.58 g/kw-h in IT100 condition.

CO is generated in rich mixture and high temperature conditions. Experimental results showed that the indicated specific CO and HC emissions increased from 151.13 and 1.98 g/kw-h to 188.67 and 5.04 g/kW-h respectively when injection timing was retarded from 300 to 100 CAD BTDC, as shown in Fig. 3. This is mainly caused by the poor mixing (Fig. 6) and wall-wetting (Fig. 7) of late EDI injection. Fig. 12 shows the distribution of CO concentration at EVO from simulation. It can be seen that the left region in the combustion chamber has the highest CO formation rate. This is because the mixture in these regions is richer than the stoichiometric equivalence ratio and there is not enough oxygen for a complete burning (Fig. 6). Consequently CO is generated in incomplete combustion. The CO concentration is higher in late EDI injections (IT180 and IT100) than that in early EDI injection (IT300) due to the uneven mixture (Figs. 6 and 10). Moreover, there are more liquid fuel droplets (Fig. 10) and wall-film (Fig. 7) in IT180 and IT100 conditions than that in IT300 condition. These will also contribute to the increased CO and HC emissions of late EDI timing conditions.

3.4. Reducing wall wetting and incomplete combustion by decreasing the ratio of fuel directly injected

In the original proposal of EDI [57], only a small proportion of ethanol fuel was used to significantly reduce the consumption of gasoline fuel in SI engines by implementing engine downsizing technologies. This sub-section aims to numerically investigate the potential of direct injection of small amount of ethanol fuel on reducing the wall-wetting and incomplete combustion at late EDI timing at 100 CAD BTDC. Fig. 13 shows the distributions of equivalence ratio and wall film height of 46% (E46), 25% (E25) and 10% (E10) of EDI at spark timing of 15 CAD BTDC. As shown in Fig. 13, the equivalence ratio around the spark plug increases due to the increase of gasoline vapour with the decrease of the proportion of ethanol fuel. This should lead to readier ignition and consequently faster combustion. Meanwhile, the fuel impingement on the piston and cylinder walls becomes much less with smaller amount of EDI. The calculated wall-film mass reduces significantly from 0.733 mg in E46 to 0.330 mg in E25 and 0.071 mg in E10. This is because smaller amount of EDI requires shorter injection time, which reduces the spray penetration length and leads to less fuel impingement, resulting in reduced HC and soot emissions [58].

Fig. 14 shows the spatial distributions of unburnt mixture, ethanol droplets and cylinder temperature at the time of EVO. When the ethanol ratio is reduced from E46 to E25 and then E10, the area of unburnt mixture ($c=0$) at EVO reduces significantly and the unevaporated ethanol droplets are greatly reduced. These should reduce the over-rich mixture and over-cooling regions, as identified and discussed in Fig. 10, and consequently reduce the HC and CO emissions. As shown in Fig. 14, the local over-cooling regions with temperature lower than 400 K are reduced from E46 to E25 and eliminated at E10. Figs. 13 and 14 suggest that the fuel impingement and incomplete combustion caused by the local over-rich and over-cooling of late EDI timing can be addressed by direct injection of smaller amount of ethanol fuel, such as E25 and E10.

4. Conclusions

Ethanol direct injection plus gasoline port injection (EDI+GPI) is a new technology to utilise ethanol fuel more effectively and efficiently in SI engines by taking advantages of ethanol fuel and direct injection, such as the cooling effect and anti-knock ability. In the development of EDI+GPI, late EDI timing was desired because late EDI timing was more effective than early EDI timing on knock mitigation, but combustion and emission performance of the engine were deteriorated by late injection, as reported in previous experimental study. To understand the mechanisms behind the experimental results, a full CFD modelling was performed to investigate the mixture formation and combustion characteristics in an EDI+GPI dual-fuelled research engine considering both the port injection and direct injection sprays. The mixture was stoichiometric and ethanol/gasoline ratio was 46% by volume. The engine speed was 4000 rpm and spark timing was 15 CAD BTDC. The EDI pressure was 6.0 MPa and the GPI pressure was 0.25 MPa. The effects of injection timing on the fuel evaporation, mixing, wall-wetting, combustion and emission formation processes were investigated. Based on the understanding gained from simulation, the potential of direct injection of small amount of ethanol fuel that cannot be realised on the current research engine on reducing the wall-wetting and incomplete combustion was examined. The major results of this study can be concluded as follows.

1. When EDI timing is retarded from IT300 to IT180 and IT100, the mixture around the spark plug becomes leaner and the distribution of equivalence ratio becomes more uneven due to the slower in-cylinder flows and reduced time for ethanol fuel to evaporate and to mix with air. Moreover, the fuel impingement on cylinder and piston walls becomes severe with the retarding of EDI timing because of the reduced combustion chamber volume and gas flow rate in the compression stroke.
2. The combustion speed becomes slower because of the leaner mixture around the spark plug when EDI timing is retarded. As a result, the peak cylinder pressure and combustion temperature of IT180 and IT100 conditions are smaller than that of IT300 condition. Late EDI timing causes over-cooling effect and over-rich mixture in the region opposite the spark plug, which consequently leads to incomplete combustion.
3. The wall impingement is more significant and more fuel remains unburnt by the time of EVO when EDI timing is changed from 300 to 180 and then to 100 CAD BTDC. This explains why the HC emission increased at late EDI timing in the experimental investigation. The NO decreases with the retarding of EDI timing due to the reduced combustion temperature. The CO increases with the retarding of EDI timing due to the poor mixing process.
4. The fuel impingement and incomplete combustion caused by the local over-rich and over-cooling of late EDI timing can be addressed by reducing the ratio of ethanol fuel to an optimal point.

Acknowledgement

The scholarship provided by the China Scholarship Council (CSC) is gratefully appreciated.

Nomenclature

ABDC: After bottom dead centre

ATDC: After top dead centre

BBDC: Before bottom dead centre

BDC: Bottom dead centre

BTDC: Before top dead centre

CAD: Crank angle degree

CFD: Computational fluid dynamics

CFM: Coherent Flame Model

CI: Compression ignition

DI: Direct injection

DFSC: Dual-fuel sequential combustion

DFSI: Dual-fuel spark ignition

ECFM: Extended Coherent Flame Model

EDI+GPI: Ethanol direct injection plus gasoline port injection

EVO: Exhaust valve open

FFV: Flexible-fuel vehicle

ITNFS: Intermediate turbulent net flame stretch

IT’xxx’: Injection timing of xxx CAD BTDC

PDF: Probability Density Function

PI: Port injection

RCCI: Reactivity Controlled Compression Ignition

SI: Spark ignition

References

[1] M. Guo, W. Song, J. Buhain. Bioenergy and biofuels: History, status, and perspective. Renewable and Sustainable Energy Reviews 2015; 42: 712-725.

[2] F. Catapano, S. Di Iorio, A. Magno, P. Sementa, B.M. Vaglieco. A comprehensive analysis of the effect of ethanol, methane and methane-hydrogen blend on the combustion process in a PFI (port fuel injection) engine. Energy 2015; 88: 101-110.

[3] M.K. Balki, C. Sayin. The effect of compression ratio on the performance, emissions and combustion of an SI (spark ignition) engine fueled with pure ethanol, methanol and unleaded gasoline. Energy 2014; 71: 194-201.

[4] F. Catapano, P. Sementa, B.M. Vaglieco. Optical characterization of bio-ethanol injection and combustion in a small DISI engine for two wheels vehicles. Fuel 2013; 106: 651-666.

[5] L.C. Monteiro Sales, J.R. Sodré. Cold start characteristics of an ethanol-fuelled engine with heated intake air and fuel. Applied Thermal Engineering 2012; 40: 198-201.

[6] C. Liang, C. Ji, B. Gao, X. Liu, Y. Zhu. Investigation on the performance of a spark-ignited ethanol engine with DME enrichment. Energy Conversion and Management 2012; 58: 19-25.

[7] Y. Huang, S. Huang, R. Huang, G. Hong. Spray and evaporation characteristics of ethanol and gasoline direct injection in non-evaporating, transition and flash-boiling conditions. Energy Conversion and Management 2016; 108: 68-77.

[8] G. Karavalakis, D. Short, D. Vu, R.L. Russell, A. Asa-Awuku, H. Jung, K.C. Johnson, T.D. Durbin. The impact of ethanol and iso-butanol blends on gaseous and particulate emissions from two passenger cars equipped with spray-guided and wall-guided direct injection SI (spark ignition) engines. Energy 2015; 82: 168-179.

[9] A.N. Ozsezen, M. Canakci. Performance and combustion characteristics of alcohol–gasoline blends at wide-open throttle. Energy 2011; 36: 2747-2752.

[10] R. Suarez-Bertoa, A.A. Zardini, H. Keuken, C. Astorga. Impact of ethanol containing gasoline blends on emissions from a flex-fuel vehicle tested over the Worldwide Harmonized Light duty Test Cycle (WLTC). Fuel 2015; 143: 173-182.

[11] D. Turner, H. Xu, R.F. Cracknell, V. Natarajan, X. Chen. Combustion Performance of Bio-ethanol at Various Blend Ratios in a Gasoline Direct Injection Engine. Fuel 2011; 90: 1999-2006.

[12] B. Kegl, S. Pehan. Reduction of Diesel Engine Emissions by Water Injection. SAE International 2001-01-3259; 2001.

[13] X. Tauzia, A. Maiboom, S.R. Shah. Experimental study of inlet manifold water injection on combustion and emissions of an automotive direct injection Diesel engine. Energy 2010; 35: 3628-3639.

[14] Z. Şahin, M. Tuti, O. Durgun. Experimental investigation of the effects of water adding to the intake air on the engine performance and exhaust emissions in a DI automotive diesel engine. Fuel 2014; 115: 884-895.

[15] V. Chintala, K.A. Subramanian. Experimental investigation of hydrogen energy share improvement in a compression ignition engine using water injection and compression ratio reduction. Energy Conversion and Management 2016; 108: 106-119.

[16] R.D. Reitz. Directions in internal combustion engine research. Combustion and Flame 2013; 160: 1-8.

[17] A. Gharehghani, R. Hosseini, M. Mirsalim, S.A. Jazayeri, T. Yusaf. An experimental study on reactivity controlled compression ignition engine fueled with biodiesel/natural gas. Energy 2015; 89: 558-567.

[18] J. Benajes, S. Molina, A. García, J. Monsalve-Serrano. Effects of low reactivity fuel characteristics and blending ratio on low load RCCI (reactivity controlled compression ignition) performance and emissions in a heavy-duty diesel engine. Energy 2015; 90, Part 2: 1261-1271.

[19] L. Zhu, Y. Qian, X. Wang, X. Lu. Effects of direct injection timing and premixed ratio on combustion and emissions characteristics of RCCI (Reactivity Controlled Compression Ignition) with N-heptane/gasoline-like fuels. Energy 2015; 93, Part 1: 383-392.

[20] D.R. Cohn, L. Bromberg, J.B. Heywood, Direct Injection Ethanol Boosted Gasoline Engines: Biofuel Leveraging for Cost Effective Reduction of Oil Dependence and CO2 Emissions, in, Massachusetts Institute of Technology, Cambridge, MA 02139, 2005.

[21] T. Ikoma, S. Abe, Y. Sonoda, H. Suzuki, Y. Suzuki, M. Basaki. Development of V-6 3.5-liter Engine Adopting New Direct Injection System. SAE paper 2006-01-1259; 2006.

[22] Toyota Camry 2.0 D-4S 6AR-FSE engine specifications, http://www.gac-toyota.com.cn/minisite/campaigns/2014/camry/p/config?index=0.

[23] R.A. Stein, C.J. House, T.G. Leone. Optimal Use of E85 in a Turbocharged Direct Injection Engine. SAE Int. J. Fuels Lubr. 2009; 2: 670-682.

[24] G. Zhu, D. Hung, H. Schock. Combustion characteristics of a single-cylinder spark ignition gasoline and ethanol dual-fuelled engine. Proc. IMechE Part D: Automobile Engineering 2010; 224: 387-403.

[25] Z. Wang, H. Liu, Y. Long, J. Wang, X. He. Comparative study on alcohols–gasoline and gasoline–alcohols dual-fuel spark ignition (DFSI) combustion for high load extension and high fuel efficiency. Energy 2015; 82: 395-405.

[26] X. Wu, R. Daniel, G. Tian, H. Xu, Z. Huang, D. Richardson. Dual-injection: The flexible, bi-fuel concept for spark-ignition engines fuelled with various gasoline and biofuel blends. Applied Energy 2011; 88: 2305-2314.

[27] Y. Zhuang, G. Hong. Primary Investigation to Leveraging Effect of Using Ethanol Fuel on Reducing Gasoline Fuel Consumption. Fuel 2013; 105: 425-431.

[28] N. Kim, S. Cho, K. Min. A study on the combustion and emission characteristics of an SI engine under full load conditions with ethanol port injection and gasoline direct injection. Fuel 2015; 158: 725-732.

[29] R. Daniel, C. Wang, H. Xu, G. Tian, D. Richardson. Dual-Injection as a Knock Mitigation Strategy Using Pure Ethanol and Methanol. SAE Int. J. Fuels Lubr. 2012; 5: 772-784.

[30] H. Liu, Z. Wang, J. Wang. Methanol-gasoline DFSI (dual-fuel spark ignition) combustion with dual-injection for engine knock suppression. Energy 2014; 73: 686-693.
[31] Y. Zhuang, G. Hong. Effects of direct injection timing of ethanol fuel on engine knock and lean burn in a port injection gasoline engine. Fuel 2014; 135: 27-37.
[32] C. Jiang, X. Ma, H. Xu, S. Richardson. An Optical Study of DMF and Ethanol Combustion Under Dual-Injection Strategy. SAE paper 2012-01-1237; 2012.
[33] S. Wei, K. Ji, X. Leng, F. Wang, X. Liu. Numerical simulation on effects of spray angle in a swirl chamber combustion system of DI (direct injection) diesel engines. Energy 2014; 75: 289-294.
[34] B. Yang, M. Yao, W.K. Cheng, Y. Li, Z. Zheng, S. Li. Experimental and numerical study on different dual-fuel combustion modes fuelled with gasoline and diesel. Applied Energy 2014; 113: 722-733.
[35] S.L. Kokjohn, R.M. Hanson, D.A. Splitter, R.D. Reitz. Experiments and Modeling of Dual-Fuel HCCI and PCCI Combustion Using In-Cylinder Fuel Blending. SAE Int. J. Engines 2009; 2: 24-39.
[36] J. Li, W.M. Yang, H. An, D.Z. Zhou, W.B. Yu, J.X. Wang, L. Li. Numerical investigation on the effect of reactivity gradient in an RCCI engine fueled with gasoline and diesel. Energy Conversion and Management 2015; 92: 342-352.
[37] X. Lu, X. Zhou, L. Ji, Z. Yang, D. Han, C. Huang, Z. Huang. Experimental studies on the dual-fuel sequential combustion and emission simulation. Energy 2013; 51: 358-373.
[38] A. Paykani, A.-H. Kakaee, P. Rahnama, R.D. Reitz. Effects of diesel injection strategy on natural gas/diesel reactivity controlled compression ignition combustion. Energy 2015; 90, Part 1: 814-826.
[39] N. Ishikawa, A. Hiraide, T. Takabayashi. Air/Fuel Distribution Simulation in a Port Injected Gasoline Lean-burn Engine. SAE paper 2001-01-1230; 2001.
[40] Y. Huang, G. Hong, R. Huang. Numerical investigation to the dual-fuel spray combustion process in an ethanol direct injection plus gasoline port injection (EDI+GPI) engine. Energy Conversion and Management 2015; 92: 275-286.
[41] M. Yumoto, K. Goto, S. Kato, M. Iida. The Investigation of Mixture Formation and Combustion with Port Injection System by Visualization of Flame and Wall Film. SAE paper 2011-01-1887; 2011.
[42] L. Postrioti, F. Mariani, M. Battistoni. Experimental and numerical momentum flux evaluation of high pressure Diesel spray. Fuel 2012; 98: 149-163.
[43] X. Jiang, G.A. Siamas, K. Jagus, T.G. Karayiannis. Physical Modelling and Advanced Simulations of Gas–liquid Two-phase Jet Flows in Atomization and Sprays. Progress in Energy and Combustion Science 2010; 36: 131-167.
[44] S. Jafarmadar. Three-dimensional modeling and exergy analysis in Combustion Chambers of an indirect injection diesel engine. Fuel 2013; 107: 439-447.
[45] R.D. Reitz. Mechanisms of Atomization Processes in High-Pressure Vaporizing Sprays. Atomization and Spray Technology 1988; 3: 309-337.

[46] R. Scarcelli, T. Wallner, N. Matthias, V. Salazar, S. Kaiser. Mixture Formation in Direct Injection Hydrogen Engines: CFD and Optical Analysis of Single- and Multi-Hole Nozzles. SAE Int. J. Engines 2011; 4: 2361-2375.

[47] ANSYS FLUENT Theory Guide. 2012.

[48] A.B. Liu, D. Mather, R.D. Reitz. Modeling the Effects of Drop Drag and Breakup on Fuel Sprays. SAE paper 930072; 1993.

[49] D.W. Stanton, C.J. Rutland. Modeling Fuel Film Formation and Wall Interaction in Diesel Engines. SAE paper 960628; 1996.

[50] P.J. O'Rourke, A.A. Amsden. A Spray/Wall Interaction Submodel for the KIVA-3 Wall Film Model. SAE paper 2000-01-0271; 2000.

[51] S.S. Sazhin. Advanced models of fuel droplet heating and evaporation. Progress in Energy and Combustion Science 2006; 32: 162-214.

[52] V. Knop, A. Benkenida, S. Jay, O. Colin. Modelling of combustion and nitrogen oxide formation in hydrogen-fuelled internal combustion engines within a 3D CFD code. International Journal of Hydrogen Energy 2008; 33: 5083-5097.

[53] G. Tian, R. Daniel, H. Li, H. Xu, S. Shuai, P. Richards. Laminar Burning Velocities of 2,5-Dimethylfuran Compared with Ethanol and Gasoline. Energy & Fuels 2010; 24: 3898-3905.

[54] J.A. Miller, C.T. Bowman. Mechanism and modeling of nitrogen chemistry in combustion. Progress in Energy and Combustion Science 1989; 15: 287-338.

[55] F. Tap, P. Schapotschnikow. Efficient Combustion Modeling Based on Tabkin® CFD Look-up Tables: A Case Study of a Lifted Diesel Spray Flame. SAE paper 2012-01-0152; 2012.

[56] J.B. Heywood. Internal Combustion Engine Fundamentals. McGraw-Hill Book Company; 1988.

[57] D.R. Cohn, L. Bromberg, J. Heywood. Fuel Management System for Variable Ethanol Octane Enhancement of Gasoline Engines. US Patent 2010175659; 15 July, 2010.

[58] A. Matsumoto, W.R. Moore, M.-C. Lai, Y. Zheng, M. Foster, X.-B. Xie, D. Yen, K. Confer, E. Hopkins. Spray Characterization of Ethanol Gasoline Blends and Comparison to a CFD Model for a Gasoline Direct Injector. SAE Int. J. Engines 2010; 3: 402-425.

Table 1. Computational models.

Turbulence model	Realizable k-ε model
Primary break-up model	Rosin-Rammler Distribution Method
Secondary breakup model	WAVE model [45]
Distortion and drag	Dynamic Drag model [48]
Wall-film model	Stanton [49] and O'Rourke [50] model
Evaporation model	Convection/Diffusion Controlled model [51]
Spark model	Zimont model [47]
Combustion model	ECFM partially premixed combustion [40]
NO model	Extended Zeldovich mechanism [54]

Table 2. Engine specifications.

Engine type	Single cylinder, air cooled, four-stroke
Displacement	249.0 cc
Stroke × Bore	58.0 × 74.0 mm
Compression ratio	9.8:1
Intake valve open	22.20 CAD BTDC
Intake valve close	53.80 CAD ABDC
Exhaust valve open	54.60 CAD BBDC
Exhaust valve close	19.30 CAD ATDC
Ethanol delivery system	Direct injection
Gasoline delivery system	Port injection

Table 3. Simulated engine conditions.

Engine speed (rpm)	4000
Throttle position	36%
Ethanol/gasoline ratio	46%, 25% and 10%
Spark timing (CAD BTDC)	15
GPI pressure (MPa)	0.25
GPI timing (CAD BTDC)	410
EDI pressure (MPa)	6.0
EDI timing (CAD BTDC)	300, 180 and 100

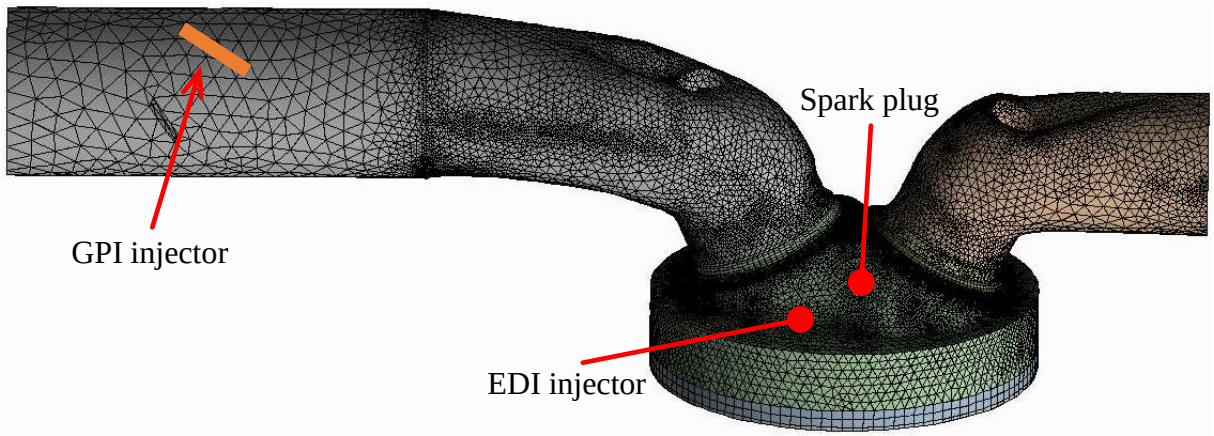

Fig. 1. Computational mesh.

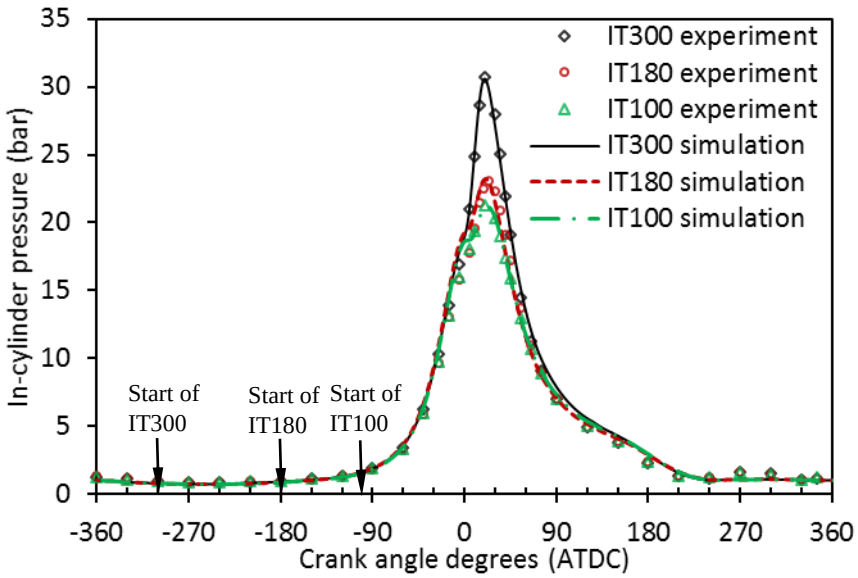

Fig. 2. Comparison of experimental and numerical in-cylinder pressure with different EDI timings.

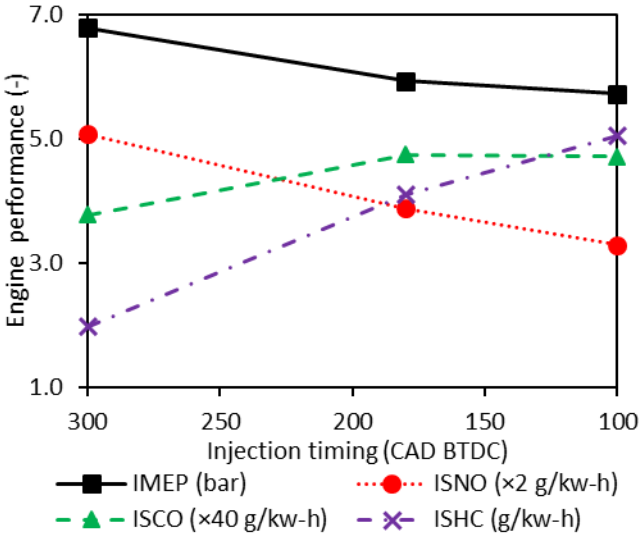

Fig. 3. Experimental results of IMEP, ISNO, ISCO and ISHC varying with EDI timing.

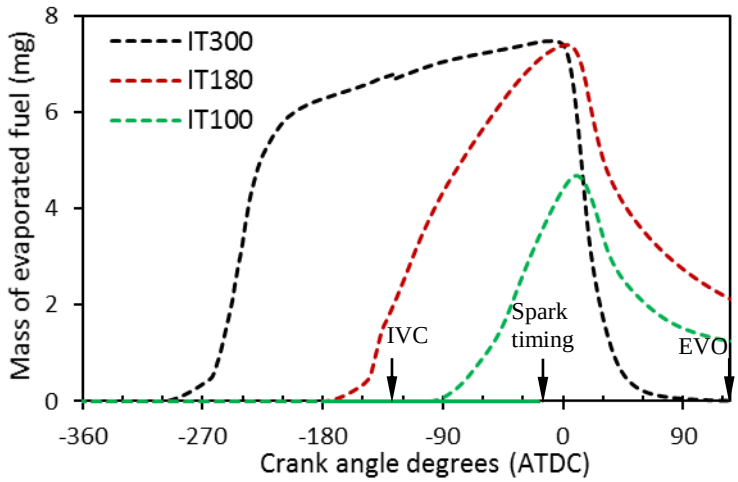

Fig. 4. Variations of mass of the vapour ethanol fuel with crank angle degrees.

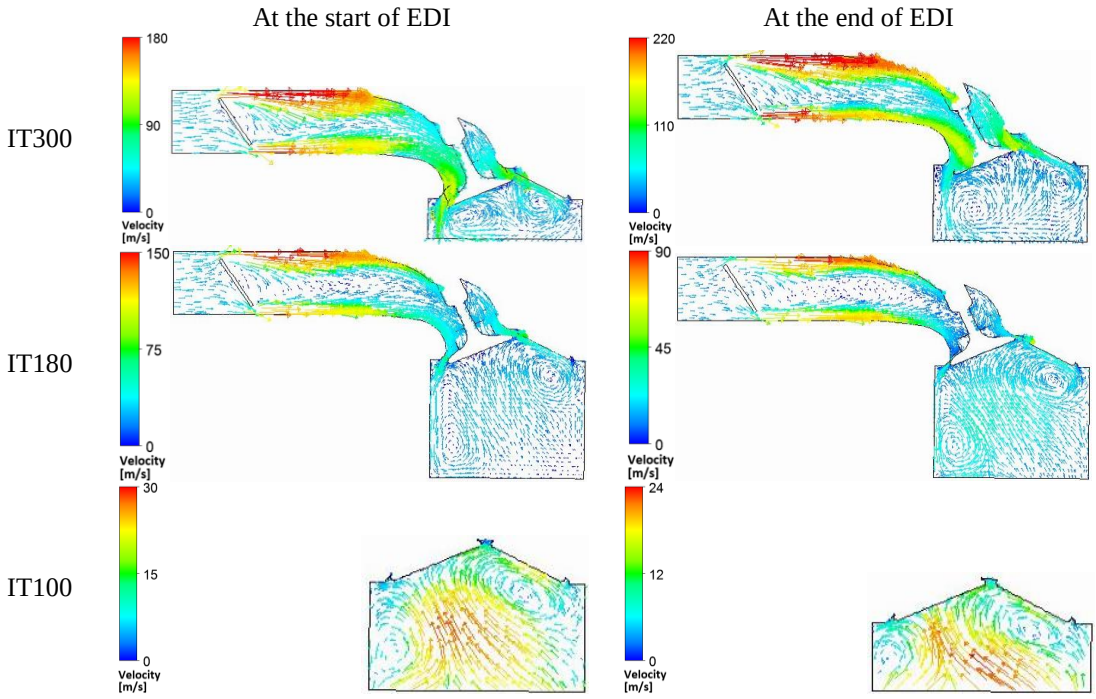

Fig. 5. Air flow velocity vectors on the engine symmetry plane at the start and end of EDI injection with different EDI timings.

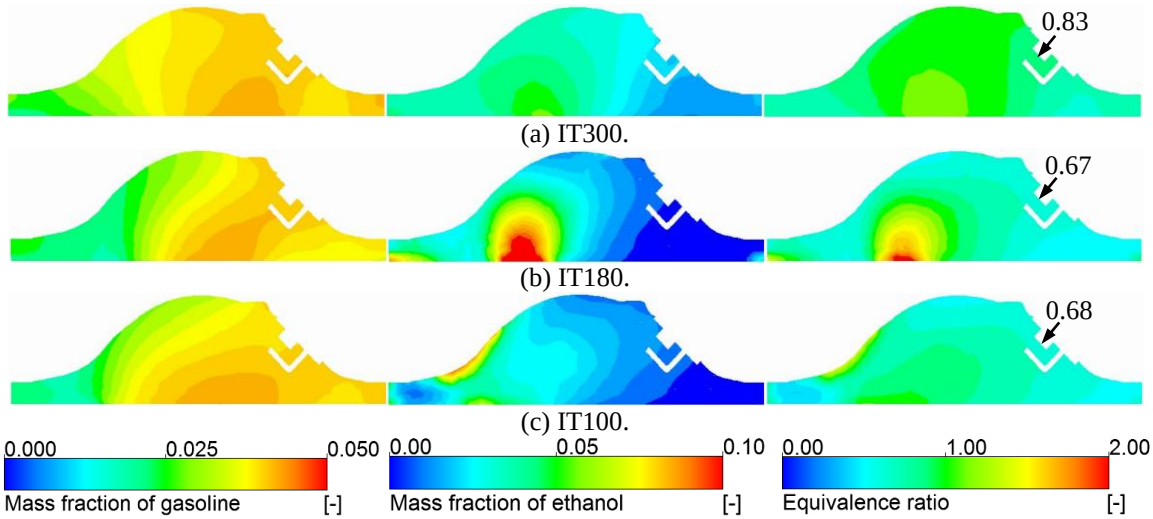

Fig. 6. Distributions of the vapour mass fractions of gasoline and ethanol fuels and the equivalence ratio on a vertical plane passing through the spark plug by spark timing.

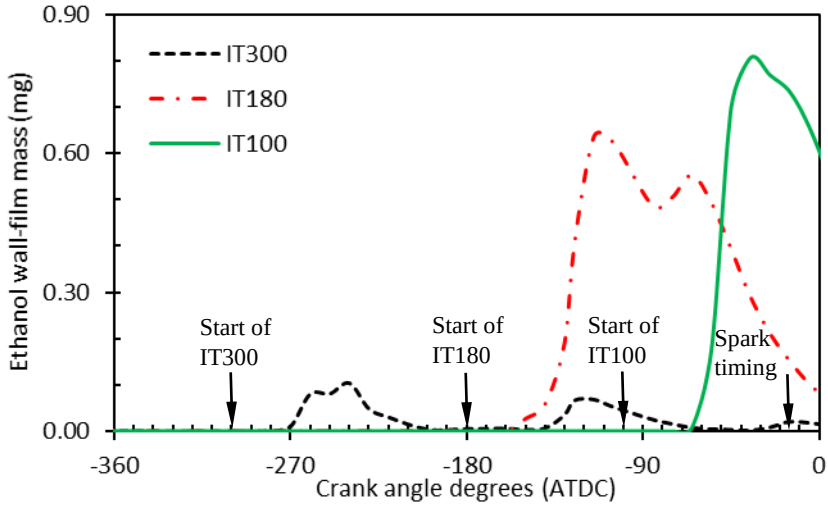

Fig. 7. Variations of wall film mass with crank angle degrees at different EDI timings.

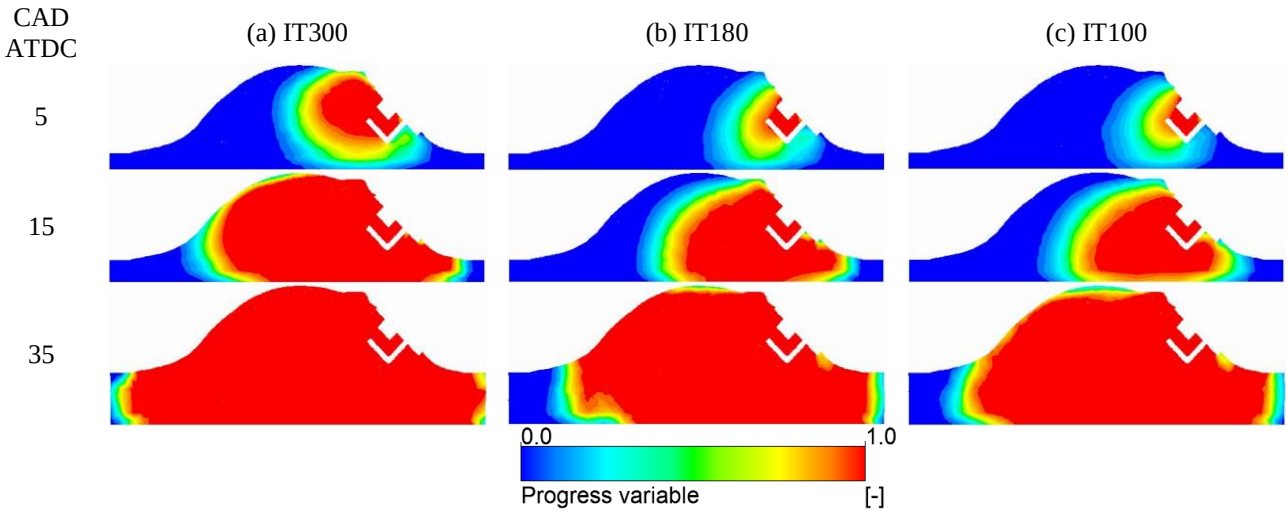

Fig. 8. Evolution of flame-brush with different EDI timings.

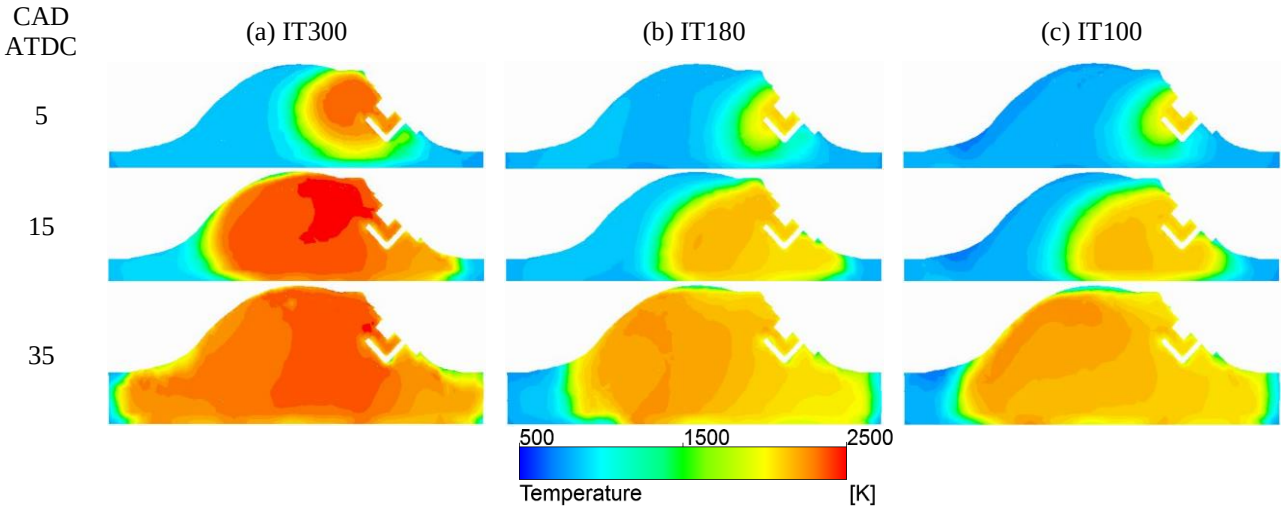

Fig. 9. Spatial distributions of combustion temperature with different EDI timings.

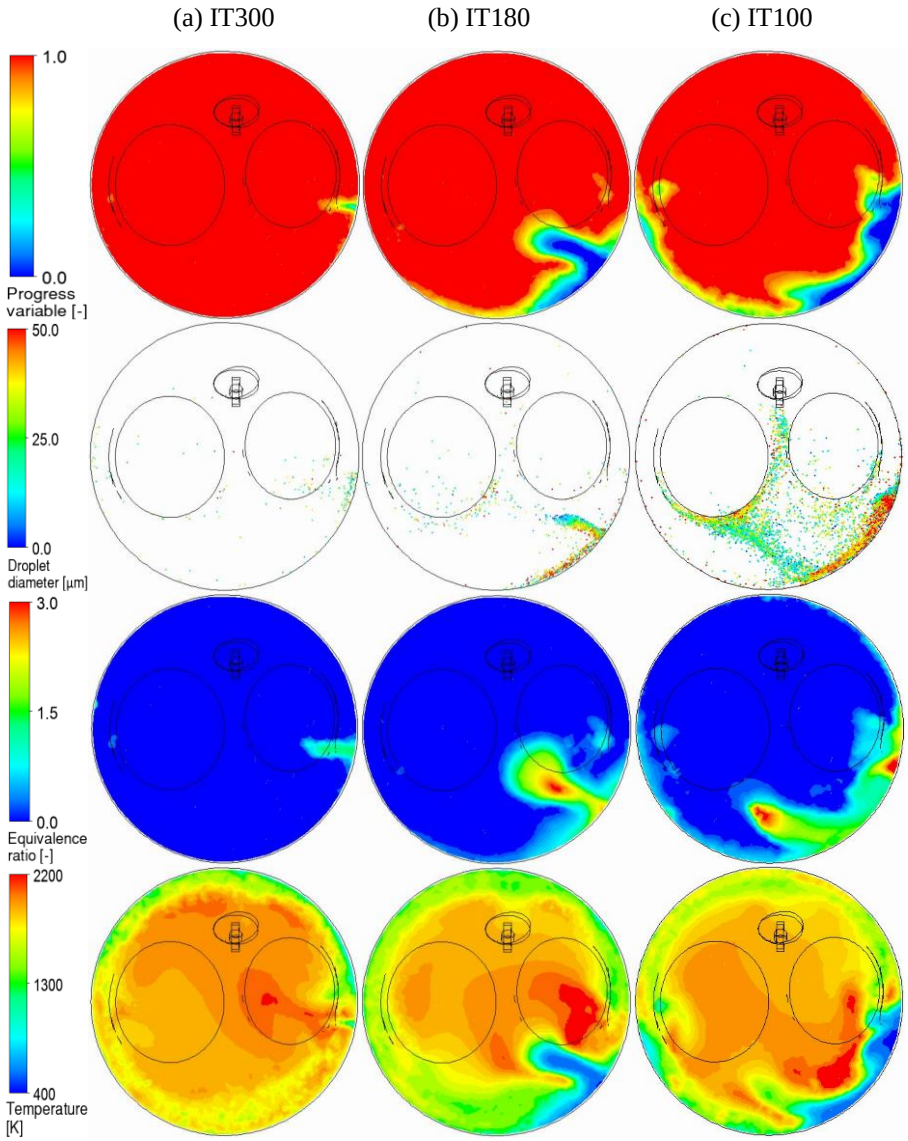

Fig. 10. Distributions of flame brush, ethanol droplets, equivalence ratio and temperature at EVO at different EDI timings.

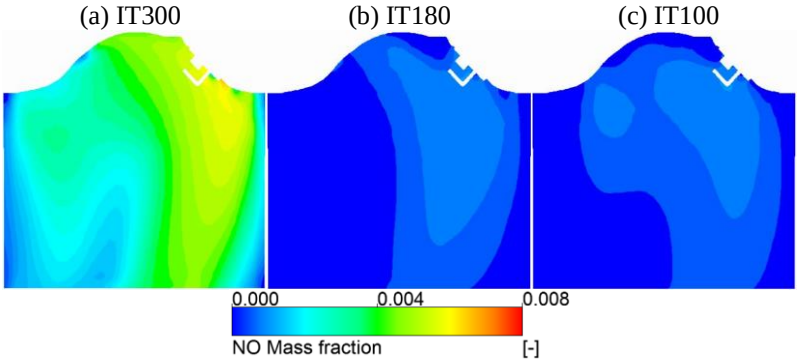

Fig. 11. Distribution of NO mass fraction at EVO.

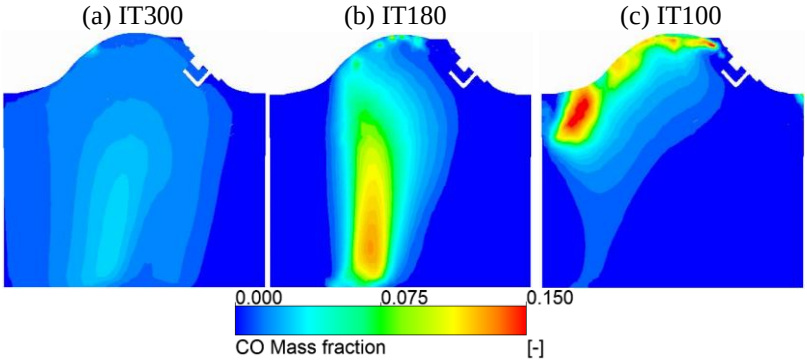

Fig. 12. Distribution of CO mass fraction at EVO.

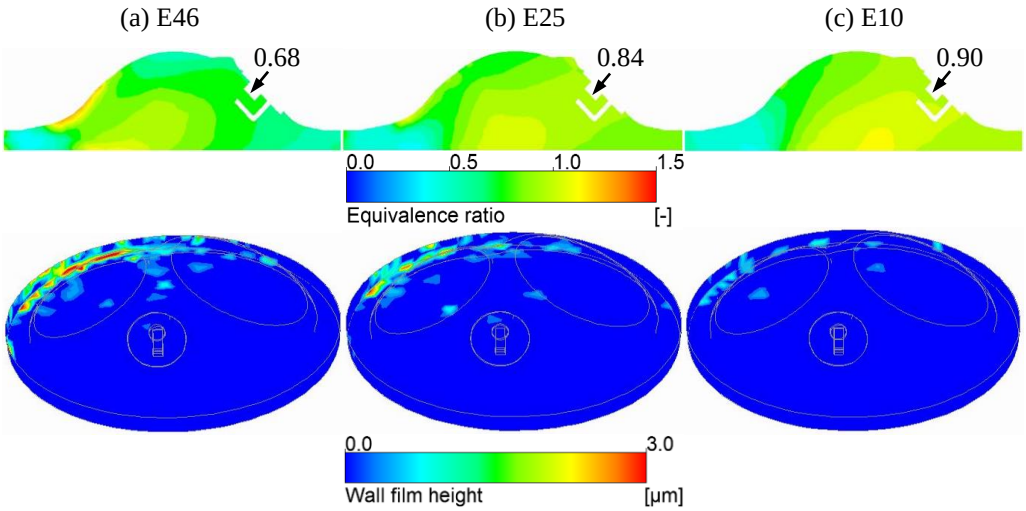

Fig. 13. Distributions of the equivalence ratio and wall film of smaller amount of ethanol fuel at IT100 by spark timing.

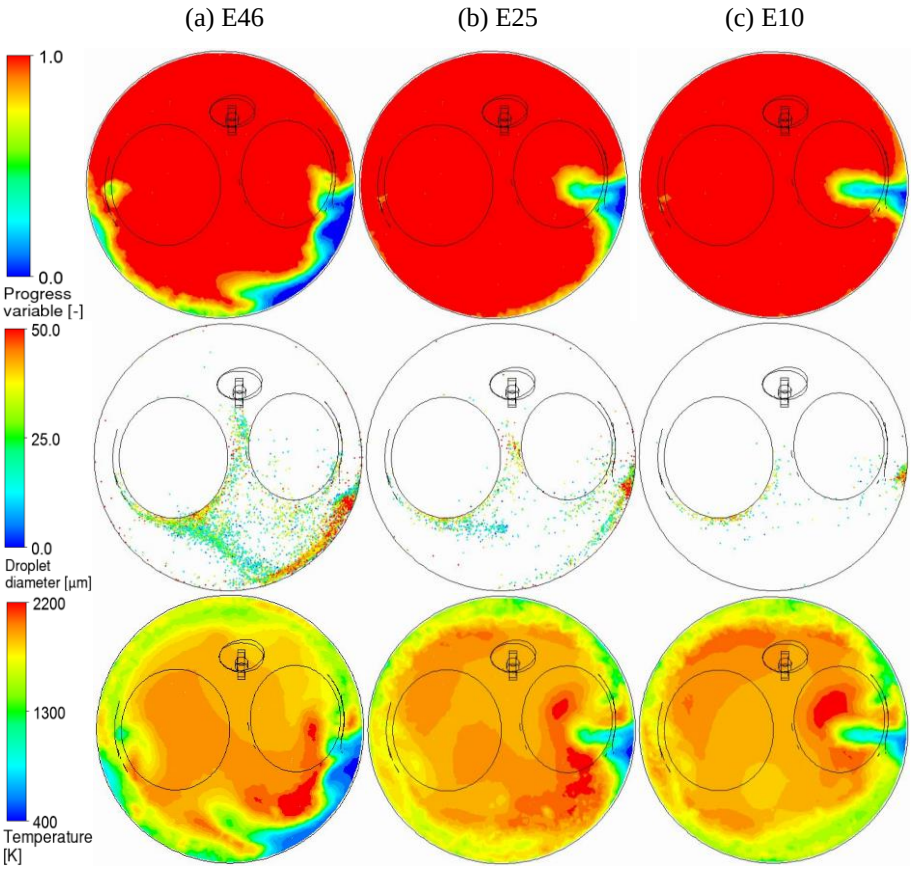

Fig. 14. Distributions of flame brush, ethanol droplets and temperature of smaller amount of ethanol fuel at IT100 at the time of EVO.